Int. J. Electrochem. Sci., 16 **(2021)** Article Number: 211237, doi: 10.20964/2021.12.35

International Journal of
ELECTROCHEMICAL
SCIENCE
www.electrochemsci.org

Electrochemical Detection of the Anesthetic Drug Procaine Hydrochloride Based on Molecularly Imprinted Polymer/Diamond-Graphite Composite Electrode

Ying Zhu[1,*], *Yang Xu*[2], *Guangxuan Liu*[1]

[1] Department of Pharmacy, Liaoning Cancer Hospital & Institute, Cancer Hospital of China Medical University, Shenyang, P.R. China
[2] Department of Pharmacy, Shenyang Orthopaedic Hospital, Shenyang, P.R. China
[*]E-mail: zhuyingpharm@163.com

Received: 15 August 2021 / *Accepted:* 7 October 2021 / *Published:* 10 November 2021

Overdose of procaine may lead to many health problems. However, highly sensitive detection of procaine has always been a challenge. Electrochemical sensor is of great significance in the field of life and health due to its high sensitivity, low cost and compatibility with portable technology. In this work, a sensor based on diamond/graphite hybrid with a molecular imprinting membrane was developed. The sp^3-bonded diamond and sp^2-bonded graphite have good mechanical properties and wide potential window. The molecular imprinting membrane can be immobilized on the diamond/graphite surface for selective determination of procaine. The optimized conditions allowed the sensor to detect the procaine concentration linearly in the range of 4×10^{-8} - 2.5×10^{-5} M. The limits of detection were calculated to be 1.5×10^{-8} M.

Keywords: Procaine; Electrochemical sensor; Diamond; Graphite; Anesthetic drug

1. INTRODUCTION

As a local anesthetic drug, procaine is commonly applied in infiltration anesthesia, block anesthesia, lumbar spine anesthesia, epidural anesthesia and local closure therapy [1–4]. In recent years, it has been found to have sedative, analgesic, antispasmodic, antiallergic, and central nervous balance restoring effects. It can also inhibit cardiac ectopic pacing point autoregulation and dilate blood vessels, thus being adopted to treat ischemic cerebrovascular disease, hemiplegia and acute renal failure [5–7]. In addition, procaine's effect of inhibiting monoamine oxidase activity can be used to delay aging as well as prevent and treat age-related diseases. However, overdose of procaine hydrochloride may result in central nervous system and cardiovascular reactions such as nausea, respiratory distress, and in severe

cases, even anaphylaxis and death. Therefore, it is important to establish a simple, efficient and sensitive analytical method for the determination of procaine [8–12].

Titration is the most commonly adopted technique for the detection of procaine. Procaine is unstable for the existence of the ester group in its chemical structure. Procaine is easily hydrolyzed and oxidized in aqueous solution, and the rate of hydrolysis is accelerated with time and temperature, producing p-aminobenzoic acid (PABA) [13–19]. The improper storage or discoloring of the solution or the aniline produced with the decarboxylation of p-aminobenzoic would not only lead to the reduction of its efficacy, but also cause the increase of the toxicity. Therefore, under the experimental conditions applied in the titration method, the hydrolysis product PABA would react with the titration solution, making the result obtained slightly higher than the true value and causing interference in the determination. In recent years, a number of reports have been made on the methods for the determination of the content of procaine [20–25]. The UV spectrophotometric method is relatively simple due to its high sensitivity and the instruments are more popular. However, the detection limit of UV spectrophotometric method is only 0.1~17μg/mL.

Electrochemical analysis has the characteristics of high sensitivity and low detection limits, thus electrochemical methods have been developed for the determination of procaine. Liu et al. [26] used differential pulse voltammetry (DPV) to determine the content of procaine and its decomposition product (PAB A). The results show that the concentration of procaine and its decomposition products (PABA) can be detected in a pH 4.50 acetate buffer solution at $5.0 \times 10\text{-}^{7}\text{-}5.0 \times 10^{-5}$ M and 5.0×10^{-7} - $2.0 \times 10\text{-}^{5}$ M. They were also successful in tracking the levels of procaine in serum and PABA in injections. Hu et al. [27] adopted pumice modified carbon paste electrodes to prepare molecularly imprinted polymers and used DPV to detect procaine in urine and drugs with linear concentrations in the range of 9.0×10^{-7} – 2.6×10^{-5} M. Despite that molecular imprinting has been proved to be an excellent choice for detecting procaine, molecular imprinting affects the conductivity of the electrode. The commonly used commercial electrodes for molecularly imprinted film modifications do not work well. Therefore, it is necessary to develop an excellent electrode for molecularly imprinted film immobilization.

Diamond/graphite composite nanomembrane is a sp^3/sp^2 carbon composite nanomaterial, which not only has the combined properties of sp^3-carbon bonded diamond and sp^2-carbon bonded graphite, but also is able to tailor the physicochemical properties of the diamond/graphite composite structure, which holds great promise for the construction of high performance electrochemical sensing electrodes. In this work, a diamond/graphite composite was prepared for molecularly imprinted film immobilization, after which the constructed composite sensor has been applied in the determination of procaine.

2. EXPERIMENTAL

2.1. Materials and instruments

(100)-oriented monocrystalline N-type silicon wafers were purchased from Hefei Kejing Material Technology Co. All the gases were purchased from Dalian Daito Gas Co. Diamond suspension was purchased from NanoCarbon Research Institute. Ltd. Acrylic acid (AA), butyl acrylate (BA),

vinyltriethoxysilane (WD-20), azobisisobutyronitrile (AIBN), glacial acetic acid, ascorbic acid, dopamine, glucose and urea were purchased from Sinopharm Chemical Reagent Co. Levodopa, epinephrine and procaine were purchased from the Chinese Institute of Pharmaceutical Biological Products.

Microwave plasma chemical vapor deposition (MPCVD) was conducted with a Iplas MPCVD. The CHI660D electrochemical workstation (Shanghai Chenhua Instruments Co., Ltd.) was used for all electrochemical experiments. A three-electrode system was adopted for testing, including a platinum wire counter electrode, an Ag/AgCl reference electrode and a molecularly imprinted polymer/diamond-graphite electrode. Raman spectrum was recorded with a Labram HR Evolution instrument (Horiba, Japan).

2.2. MPCVD of diamond/graphite (D/G) composite

The preparation of D/C composite thin films consists of three steps. In the first step, the (100)-oriented monocrystalline N-type silicon wafers were ultrasonicated for 10 min, 10 min and 3 min in the solution of propanone, ethanol and ultrapure water, respectively, and then blown dry with nitrogen for use. In the second step, clean and dry Si wafers were placed in a 0.025 w/v% diamond suspension and sonicated for 30 min. After ultrasonic crystallization, the wafers were transferred to an ethanol solution and ultrasonicated for 3 min to remove the poorly adsorbed diamond particles from the surface. In the third step, the microwave power was set to 10 kW, the chamber air pressure was set to 70 mbar, the H_2 flow rate was set to 400 sccm, and the CH_4 flow rate was varied according to the growth requirements, and the growth time was 200 min. The detailed growth preparation parameters are shown in Table 1.

Table 1. Deposition parameters and characteristic properties of D/G electrode.

Electrode	Power (kW)	CH_4 (sccm)	Gas pressure (mbar)	Substrate temperature (^oC)	Conductivity (S/cm)
D/G-1	10	28	70	1007	0.04
D/G-2		31		1110	34.07
D/G-3		35		1050	115.4

2.3. Preparation of ploy(AA-BA-WD-20) molecularly imprinted polymers and modification

AA, BA, WD-20 was added into a 250 mL quadruple-bottom flask with a certain mass ratio, after which a large amount of AIBN and anhydrous hexanol was added. Nitrogen was introduced for 15 min, and the oil bath was heated to 78.5°C with magnetic stirring. The remaining AIBN ethanol solution was then slowly added dropwise and held for 3 h to obtain a poly (AA -BA -WD-20) solution with a solid content of 15%. The molecularly imprinted polymer solution was obtained by stirring the above solution (1.5%wt) with procaine solution (20 mM) at a constant volume ratio of W for 4h at room temperature.

A certain amount of molecularly imprinted polymer solution was applied dropwise to the D/G surface and left at room temperature for 12 h. Afterwards, the modified electrodes were placed in an oven overnight. Finally, the resulting electrode was removed from the procaine molecules in the eluent to obtain the molecularly imprinted electrochemical sensor. The final sensor was denoted as D/G-x-P, where x is the sample number in Table 1.

3. RESULTS AND DISCUSSION

Figure 1 shows the SEM diagram of the change of D/G morphology with methane concentration. It can be noted that D/G-1 is composed of nanocrystals, and most of the grains are smaller than 100 nm in size. As the concentration of CH_4 increases, the surface morphology of the film changes significantly, and some nanosheet-like structures could be seen sprouting on the surface of the film. As the concentration of CH_4 increases, the length and density of the nanosheets increase continuously, and the roughness of the film surface also increases continuously [28].The sp^3-to-sp^2 conversion process for graphite growth on the surface of diamond is due to the surface carbon atoms on diamond underwent rearrangement, resulting in a conductive layer. The chemical compositions of the diamond surface before and after thermal treatment were analyzed by examine changes in the carbon bonding structure. The pristine diamond is composed of all sp^3 bonds. However, by our proposed growth process, the proportion of sp^2 bonds (C=C) increased and that of sp^3 bonds (C–C) is halved, suggesting the conversion into sp^2-bonded carbon allotropes. It is widely recognized that defects (like nitrogen-related centers) associated with the method of synthesis are incorporated in the diamond. At high temperature, the unsaturated carbon bonds at the defect sites dissolve into and diffuse on the air. The carbon bond decomposition intrinsically etches the diamond surface, which is especially pronounced along the defect boundaries. The carbon atoms diffusing on the air would coalesce and precipitate to form graphite layers at the interface between air and diamond. When the graphite layer extends and finally covers the entire diamond surface during growth, the catalytic reaction terminates because the diamond surface is isolated from the air by the graphite itself.

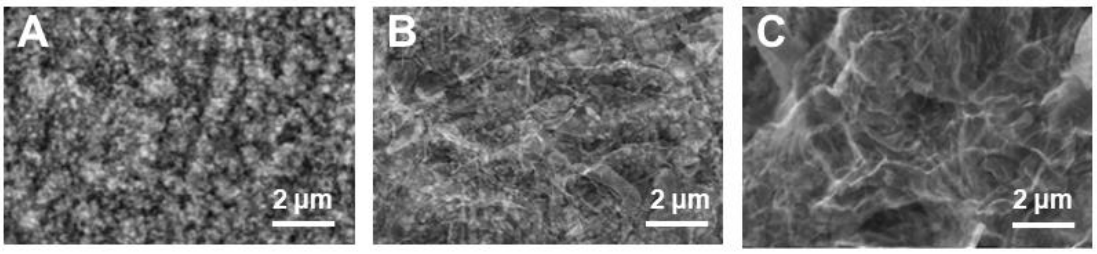

Figure 1. SEM images of D/G-1, D/G-2 and D/G-3.

Figure 2 presents the Raman spectra obtained under the 325 nm laser. The Raman spectra of all the D/G composite electrodes show significant T_{2g} peaks at 1,332 cm^{-1}, indicating the presence of the

aventurine phase in the films [29]. In addition, significant D- and G-peak signals could also be observed in the Raman spectra. The T_{2g} Raman peak broadens and the G Raman peak sharpens with the increase of the CH_4 concentration. The ratio of $I_{diamond}/I_G$ and I_D/I_G decreases with the increase of methane concentration, indicating that the phase content and crystalline quality of the graphite phase in the composite electrode are increasing.

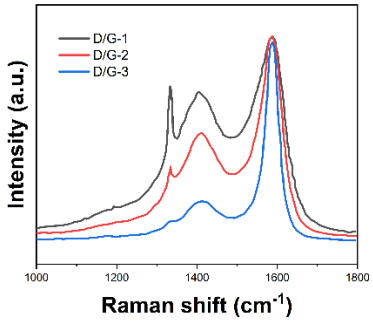

Figure 2. Raman spectra of D/G-1, D/G-2 and D/G-3 recorded using a 325 nm laser.

As an electrochemical sensing electrode, the electrochemical potential window is a key factor affecting the performance of the electrode [30]. In order to evaluate and compare the electrochemical potential window D/G electrodes in 0.1 M H_2SO_4 solution, their cyclic voltammetric response was measured. As shown in Figure 3, the cyclic voltammetric curve of D/G-1 is close to a straight line due to the low electrical conductivity of the film and the very limited electrochemical activity sites on the surface of the thin film. As the methane concentration increases, significant oxygen-dissociation and hydrogen-dissociation currents appear on both sides of the cyclic voltammetric curves of D/G-2 and D/G-3 [31]. It can be seen that the electrochemical potential window of D/G-2 is better than that of D/G-3. Therefore, D/G-2 has been selected for electrochemical sensing.

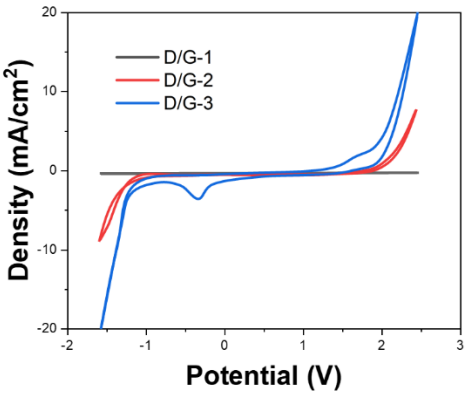

Figure 3. Cyclic voltammetry curves of D/G-1, D/G-2 and D/G-3 recorded at 0.1 M H_2SO_4.

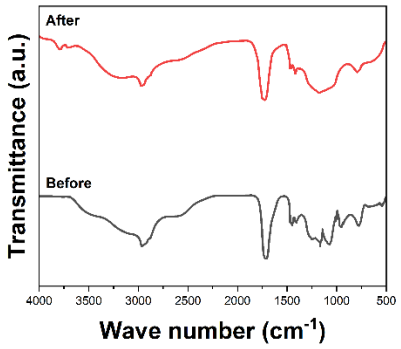

Figure 4. FTIR spectra of poly(AA-BA-WD-20) before and after solidification.

In this experiment, the polymer solution was prepared by free radical polymerization. WD-20 was applied as a siloxane coupling agent and was hydrolyzed to Si-OH and ethanol molecules upon encountering water Si-O-CH_2CH_3 group [32]. Si-OH was dehydrated and condensed with Si-OH to form Si-O-Si bonds. The FTIR plots in Figure 4 reveals that the characteristic IR absorption peak of C=C double bond in the range of 1620-1680 cm^{-1} has no absorption, indicating that the polymer solution is completely reacted without monomer remains [33]. Meanwhile, the characteristic absorption peak of C=O is around 1720 cm^{-1}, and the transmittance of its C=O characteristic peak does not change with the increase of cross-linking for the same polymer. Moreover, the Si-O-C and Si-OH groups are gradually converted to Si-O-Si groups with the increase of cross-linking [34].

AA is a functional monomer that provides hydroxyl functional groups to bond with the amino-chlorine hydrogen bonds on the target molecule, and WD-20 is a cross-linking agent, the dosage of which has a direct effect on the number of cavities [35]. The flexibility of the film can be adjusted by changing the amount of BA. The excessively low amount of AA can lead to the great reduction of the number of binding sites to which the target molecule can bind. When the dosage of WD-20 is too small, the number of fixable cavities after elution decreases, and when the amount of BA is extremely high or low, the polymer film would be extremely hard or soft, thus the formed cavities are easily destroyed or deformed, which affects the blotting effect [36]. The different polymer solutions (wt = 15%) and procaine ethanol solution (20 mM) were mixed and homogenized in a 4:1 volume ratio and finally solidified on D/G [37]. After elution, the solution was incubated in PBS buffer at pH 7.4. Figure 5A-B shows the current values that were measured. When the amount of AA remains unchanged, the blotting effect increases with the amount of WD-20 within a certain range, and the blotting effect decreases as the amount of WD-20 increases. The reason for this phenomenon is that the amount of cavities fixed after elution increases as the crosslinking degree increases within a certain range. When the crosslinking degree continues to increase, the hardness of the polymerization film increases and the polymerization film is prone to rupture in the process of elution and incubation, resulting in the destruction of some of the traced cavities and a decrease in the tracing effect of the sensor. The number of binding sites increases within a certain range as the amount of AA increases in the case that the ratio of AA:WD-20 remains unchanged. As a result, the affinity of the sensor to the target molecule increases, thus the blotting effect of the sensor increases [38]. As the amount of AA continues to increase, the hydrophilic property of the

polymeric film becomes excessively strong and the flexibility in water increases. Some of the imprinted cavities are deformed, the solvent resistance of the sensor decreases and the imprinting effect also decreases [39]. Therefore, the polymer solution with a mass ratio of AA:BA:WD-20 of 10:4:6 was selected as the best monomer mass ratio for the polymer solution.

Eluents vary in their effects on the elution of the target material encapsulated inside the highly cross-linked polymeric membrane. In addition, polymeric membranes have a certain degree of solvent resistance. The template molecules are easily eluted off with an extremely high eluent concentration, however, the membrane is also easily damaged, thus it is significant to optimize different eluents in order to achieve a better elution effect without damaging the integrity of the polymer membrane [40]. Figure 5C-F presents the relationship between the elution time and the peak current of the remaining procaine molecules in the sensor after the elution in different eluents. As shown in the figure, the elution of eluent A is complete at 20 min. The B and C eluates reach an equilibrium at about 45 min, and some peak currents remain after elution, which could not completely elute procaine from the blotted polymer membrane. Therefore, eluent A was selected for the next experiment.

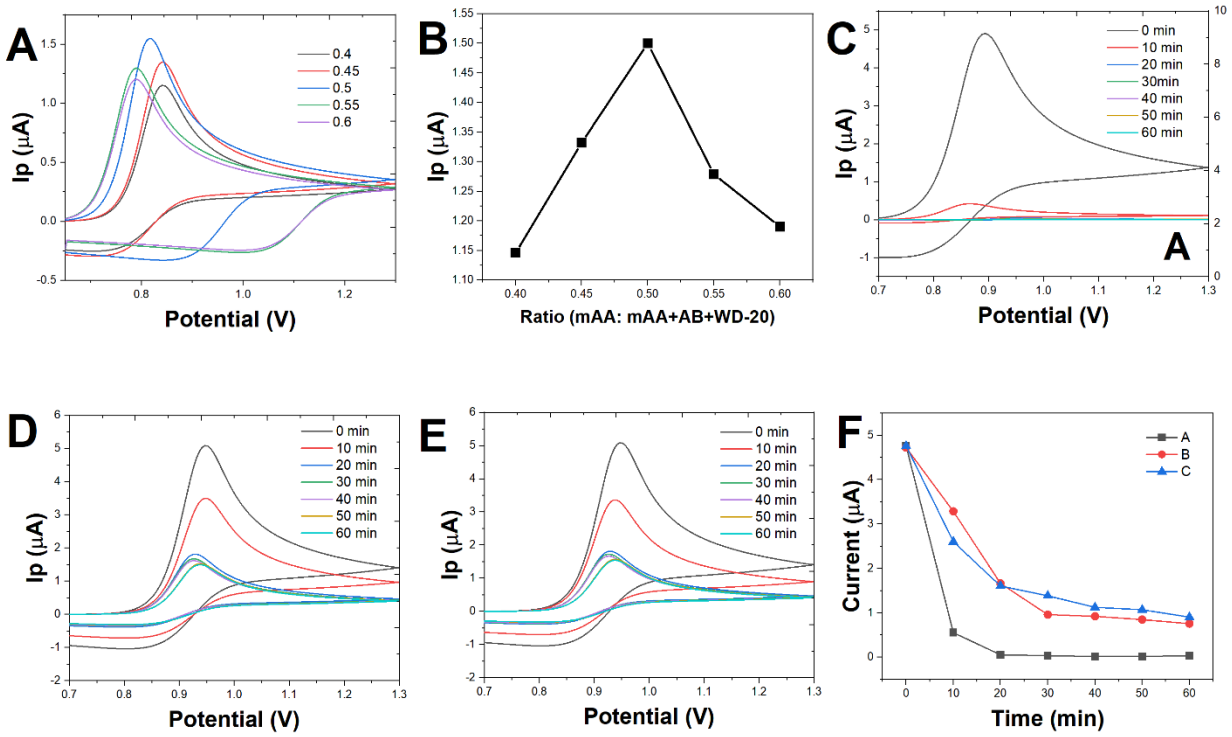

Figure 5. (A) CVs and (B) Effect of polymer monomer ratio on the effect of procaine blotting. (C-E) CVs and (E) Correlation between elution time and peak current of D/G-2-P in different eluents (A: v_{etanol}: v_{water}: $v_{acetic\ acid}$ = 3:6:1; B: v_{etanol}: v_{water} = 4:6; C: water).

Electrochemical sensors study the electrochemical signal of procaine through the hydrogen bonding of the carboxyl group to procaine on the sensor, and then detect the procaine content on the sensor. The pH of the culture medium is closely related to the ability of the sensor to bind procaine. Therefore, it is of great importance to optimize the pH of the incubation medium for blotting procaine

with electrochemical sensors in different pH buffers after elution and removal of the template molecule procaine [41]. Figure 6 shows the results of DPV scanning measurements of procaine hydrochloride oxidation peak currents after blotting adsorption of the sensor at different pH values of 16 μM procaine.

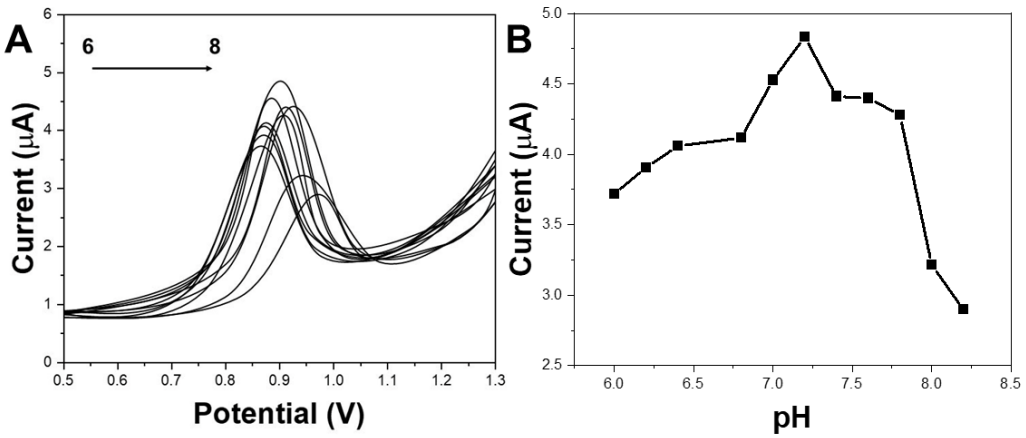

Figure 6. DPV scanning of electrochemical signals after incubation of the D/G-2-P in different pH values of the culture medium.

It can be noted from Figure 6 that the procaine oxidation peak potential shifts negatively with the increase of pH, and the affinity of the imprinted polymer for procaine is greatest when incubated at pH 7.0, with the highest peak current value. The possible reason for this phenomenon is that under acidic conditions, the hydrogen ions bind to the amino functional group of procaine, weakening the interaction between the imprinted polymer and the amino group. Under alkaline conditions, the carboxyl group and the hydroxide ion of the imprinted polymer bind. The hydrogen bonding between the carboxyl ion and the amino group decreases, and the hydrogen bonding between the imprinted polymer and the procaine decreases, leading to the decrease of the procaine oxidation peak current.

Table 2. Comparative performance data of analytical methods for procaine determination.

Method	LDR	LOD	Reference
HPLC	0.05 - 5.0 μg/mL	-	[42]
CV	5×10^{-6} - 2×10^{-4} M	0.5×10^{-6} M	[43]
DPV	9×10^{-7} – 2.6×10^{-5} M	5×10^{-8} M	[44]
UV-vis	1×10^{-7} - 1×10^{-6} M	3.8×10^{-8} M	[45]
SERS	1×10^{-8} - 1×10^{-3} M	1.5×10^{-10} M	[46]
D/G-2-P	4×10^{-8} - 2.5×10^{-5} M	1.5×10^{-8} M	This work

Under the optimized experimental conditions, the D/G-2-P was incubated in different concentrations of procaine culture solution and the relationship between the procaine concentration and its oxidation peak current was investigated by differential pulse voltammetry. As shown in Figure 7A,

the oxidation peak current increases with the procaine concentration in the culture medium. The results indicate (Figure 7B) that the peak current of procaine incubation on this electrochemical sensor is related to the concentration. A positive linear relationship was observed in the range of 4×10^{-8} - 2.5 $\times10^{-5}$ M. The limits of detection were calculated to be 1.5×10^{-8} M. Table 2 compares the analytical performance of the prepared sensor and other procaine sensing methods. The comparison shows that D/G-2-P has a wider linear range and lower detection limit when measuring procaine.

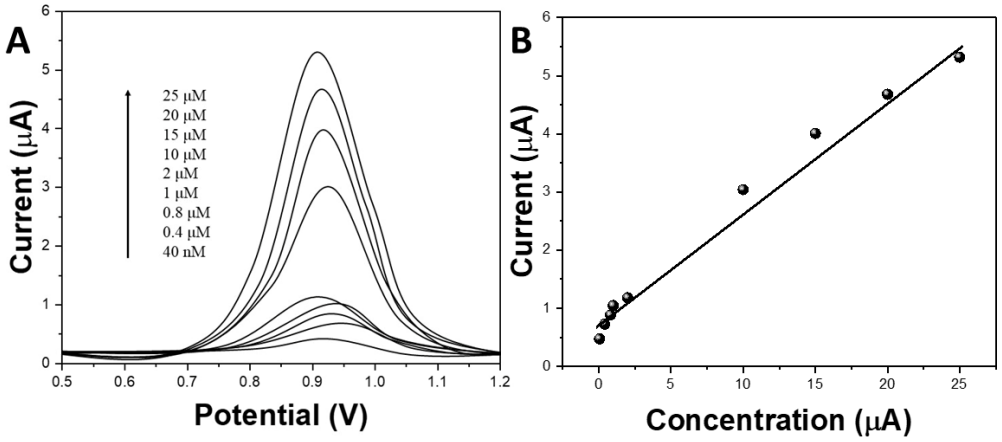

Figure 7. (A) DPV curves of the D/G-2-P towards 40 nM, 0.4 μM, 0.8 μM, 1 μM, 2 μM, 10 μM, 15 μM, 20 μM, 25 μM of procaine. (B) Plots of procaine concentration with current.

To ensure the practicality and accuracy of the D/G-2-P, the sensors must be reproducible and stable. In this experiment, three different sensors were adopted to detect and observe the stability of procaine. The results reveal that the reproducibility is good within the experimental error range. For the same sensor, the relative standard deviations of the peak current signals were 3.5%, 4.1%, 2.5%, 3.3% and 4.7%, respectively for the six measurements. The experimental results show that the D/G-2-P has good reproducibility and stability, which is practical and accurate.

To evaluate the selectivity of D/G-2-P for procaine in complex samples, chemical substances that may be present in the procaine assay environment were selected as interfering substances. Glucose, urea, dopamine, levodopa, epinephrine and ascorbic acid were also selected as interferents. The results reveal that glucose at 200-fold, urea at 100-fold, ascorbic acid at 50-fold, levodopa at 40-fold and epinephrine at 20-fold can affect the determination of procaine. Therefore, the proposed D/G-2-P has an excellent anti-interference property.

The applicability of this procaine sensor was performed after determining the procaine concentration in real samples (chicken serum). Fresh chicken blood was collected from the local market. Using EDTA as an anticoagulant, the fresh chicken blood was centrifuged to obtain a chicken serum sample. The chicken serum sample was diluted 100 times with 0.1 M NaOH solution The procaine recovery experiment in the chicken serum sample was carried out by the standard addition method. The

results are shown in Table 3. The results show that the obtained sensor has good accuracy and precision, and proves that the prepared sensor has practical application value.

Table 3. Determination of procaine in the real samples

Sample No.	Found (μM)	Added (μM)	Found (μM)	Recovery (%)	RSD (%)
1	-	2.00	2.04	102.00	3.12
2	-	5.00	4.88	97.60	2.22
3	-	10.00	10.71	107.10	2.57

4. CONCLUSION

In this study, D/G-2-P was proposed for determination of procaine. The optimized conditions allowed the sensor to detect the procaine concentration linearly in the range of 4×10^{-8} - 2.5×10^{-5} M. The limits of detection were calculated to be 1.5×10^{-8} M. In conclusion, the constructed electrochemical has a good accuracy, high sensitivity, acceptable stability and favorable reusability.

References

1. M. de Jong, N. Sleegers, A. Florea, J. Van Loon, A.L.N. van Nuijs, N. Samyn, K. De Wael, *Anal. Chem.*, 91 (2019) 15453–15460.
2. Y. Xia, L. Wu, Y. Hu, Y. He, Z. Cao, X. Zhu, X. Yi, J. Wang, *Biosensors and Bioelectronics*, 126 (2019) 269–274.
3. R. Duan, X. Fang, D. Wang, *Frontiers in Chemistry*, 9 (2021) 361.
4. C. Li, F. Sun, *Frontiers in Chemistry*, 9 (2021) 409.
5. I. Abdulazeez, S.A. Popoola, T.A. Saleh, A.A. Al-Saadi, *Chemical Physics Letters*, 730 (2019) 617–622.
6. S. Pysarevska, S. Plotycya, L. Dubenska, *Null*, 51 (2021) 339–352.
7. J. Li, S. Zhang, L. Zhang, Y. Zhang, H. Zhang, C. Zhang, X. Xuan, M. Wang, J. Zhang, Y. Yuan, *Frontiers in Chemistry*, 9 (2021) 339.
8. M. Haroon, I. Abdulazeez, T.A. Saleh, A.A. Al-Saadi, *Electrochimica Acta*, 387 (2021) 138463.
9. J. Panić, A. Tot, P. Drid, S. Gadžurić, M. Vraneš, *European Journal of Pharmaceutical Sciences*, 166 (2021) 105966.
10. J. Zhou, Y. Zheng, J. Zhang, H. Karimi-Maleh, Y. Xu, Q. Zhou, L. Fu, W. Wu, *Analytical Letters*, 53 (2020) 2517–2528.
11. H. Karimi-Maleh, Y. Orooji, F. Karimi, M. Alizadeh, M. Baghayeri, J. Rouhi, S. Tajik, H. Beitollahi, S. Agarwal, V.K. Gupta, *Biosensors and Bioelectronics* (2021) 113252.
12. W. Li, W. Luo, M. Li, L. Chen, L. Chen, H. Guan, M. Yu, *Frontiers in Chemistry*, 9 (2021) 610.
13. H. Karimi-Maleh, M. Alizadeh, Y. Orooji, F. Karimi, M. Baghayeri, J. Rouhi, S. Tajik, H. Beitollahi, S. Agarwal, V.K. Gupta, S. Rajendran, S. Rostamnia, L. Fu, F. Saberi-Movahed, S. Malekmohammadi, *Ind. Eng. Chem. Res.*, 60 (2021) 816–823.
14. K. Hao, S. Suryoprabowo, S. Song, L. Liu, Q. Zheng, H. Kuang, *Null*, 29 (2018) 1150–1161.
15. S. Plotycya, O. Strontsitska, S. Pysarevska, M. Blazheyevskiy, L. Dubenska, *International Journal of Electrochemistry*, 2018 (2018) 1376231.

16. L. Fu, W. Su, F. Chen, S. Zhao, H. Zhang, H. Karimi-Maleh, A. Yu, J. Yu, C.-T. Lin, *Bioelectrochemistry* (2021) 107829.
17. L. Fu, Y. Zheng, P. Zhang, H. Zhang, M. Wu, H. Zhang, A. Wang, W. Su, F. Chen, J. Yu, W. Cai, C.-T. Lin, *Bioelectrochemistry*, 129 (2019) 199–205.
18. Y. Xu, Y. Lu, P. Zhang, Y. Wang, Y. Zheng, L. Fu, H. Zhang, C.-T. Lin, A. Yu, *Bioelectrochemistry*, 133 (2020) 107455.
19. Y. Wang, L. Chen, T. Xuan, J. Wang, X. Wang, *Frontiers in Chemistry*, 9 (2021) 569.
20. H. Karimi-Maleh, A. Ayati, R. Davoodi, B. Tanhaei, F. Karimi, S. Malekmohammadi, Y. Orooji, L. Fu, M. Sillanpää, *Journal of Cleaner Production*, 291 (2021) 125880.
21. Z. Wu, J. Liu, M. Liang, H. Zheng, C. Zhu, Y. Wang, *Frontiers in Chemistry*, 9 (2021) 208.
22. S. Yan, Y. Yue, L. Zeng, L. Su, M. Hao, W. Zhang, X. Wang, *Frontiers in Chemistry*, 9 (2021) 220.
23. Z. Xu, M. Peng, Z. Zhang, H. Zeng, R. Shi, X. Ma, L. Wang, B. Liao, *Frontiers in Chemistry*, 9 (2021) 683.
24. Y. Yue, L. Su, M. Hao, W. Li, L. Zeng, S. Yan, *Frontiers in Chemistry*, 9 (2021) 479.
25. Y.F. Zhuang, G.P. Cao, J.Y. Mao, B.L. Liu, *Journal of Applied Spectroscopy*, 85 (2019) 1094–1100.
26. C.Y. Wang, X.Y. Hu, G. Di Jin, Z.Z. Leng, *Journal of Pharmaceutical and Biomedical Analysis*, 30 (2002) 131–139.
27. A.-L. Liu, J.-D. Wang, W. Chen, X.-H. Xia, Y.-Z. Chen, X.-H. Lin, *Journal of Solid State Electrochemistry*, 16 (2012) 1343–1351.
28. X. Peng, T. Hu, T. Bao, L. Zhao, X. Zeng, W. Wen, X. Zhang, S. Wang, *Journal of Electroanalytical Chemistry*, 799 (2017) 327–332.
29. D.A. Al-Eryani, W. Ahmad, G.I. Mohammad, F.M. Ali Zainy, H. Alwael, S.O. Bahaffi, M.S. El-Shahawi, *Journal of Fluorescence*, 29 (2019) 211–219.
30. T.R. Fiorentin, A.J. Krotulski, D.M. Martin, T. Browne, J. Triplett, T. Conti, B.K. Logan, *Journal of Forensic Sciences*, 64 (2019) 888–896.
31. G. Savaroğlu, E. Ocak, E. Hür, *Journal of Molecular Liquids* (2021) 116867.
32. C.H. Rodrigues, J.E. Hernández-González, N.J. Pedrina, V.B. Leite, A.T. Bruni, *Journal of the Brazilian Chemical Society*, 32 (2021) 800–810.
33. A.A. Al-Saadi, M. Haroon, S.A. Popoola, T.A. Saleh, *Sensors and Actuators B: Chemical*, 304 (2020) 127057.
34. M. Haroon, W. Iali, A.A. Al-Saadi, *Spectrochimica Acta Part A: Molecular and Biomolecular Spectroscopy*, 263 (2021) 120223.
35. X. Tian, Q. Fan, J. Guo, Q. Yu, L. Xu, X. Kong, *Spectrochimica Acta Part A: Molecular and Biomolecular Spectroscopy*, 263 (2021) 120174.
36. Y. Zheng, J. Zhu, L. Fu, Q. Liu, *Int. J. Electrochem. Sci*, 15 (2020) 9622–9630.
37. L. Fu, K. Xie, Y. Zheng, L. Zhang, W. Su, *Electronics*, 7 (2018) 15.
38. G. Liu, X. Yang, H. Zhang, L. Fu, *Int. J. Electrochem. Sci*, 15 (2020) 5395–5403.
39. J. Ying, Y. Zheng, H. Zhang, L. Fu, *Revista Mexicana de Ingeniería Química*, 19 (2020) 585–592.
40. R. Yang, B. Fan, S. Wang, L. Li, Y. Li, S. Li, Y. Zheng, L. Fu, C.-T. Lin, *Micromachines*, 11 (2020) 967.
41. W. Wu, M. Wu, J. Zhou, Y. Xu, Z. Li, Y. Yao, L. Fu, *Sensors and Materials*, 32 (2020) 2941–2948.
42. W. Qin, Z. Jiao, M. Zhong, X. Shi, J. Zhang, Z. Li, X. Cui, *Journal of Chromatography B*, 878 (2010) 1185–1189.
43. M. Wei, Y. Zhou, J. Zhi, D. Fu, Y. Einaga, A. Fujishima, X. Wang, Z. Gu, *Electroanalysis*, 20 (2008) 137–143.
44. C.Y. Wang, X.Y. Hu, G.D. Jin, Z.Z. Leng, *Journal of Pharmaceutical and Biomedical Analysis*, 30 (2002) 131–139.

45. Y.-H. Chen, F.-S. Tian, M.-P. Song, *Journal of Analytical Chemistry*, 64 (2009) 366–370.
46. A.A. Al-Saadi, M. Haroon, S.A. Popoola, T.A. Saleh, *Sensors and Actuators B: Chemical*, 304 (2020) 127057.